

Co-culturing of the Hepatocytes with the Endothelial and Stellate Cells within Decellularized Scaffolds by Sodium Lauryl Ester Sulfate- Approach to Tissue Constructs for Future Transplantation

L. Talebi¹, T. Talaei-Khozani²,
Z. Khodabandeh^{3*},
M. Vasaghi-Gharamaleki⁴,
Z. Vojdani^{2*}, F. Masjedi⁵

¹Student Research Committee, Shiraz University of Medical Sciences, Shiraz, Iran

²Department of Anatomy, School of Medicine, Shiraz University of Medical Sciences, Shiraz, Iran

³Stem Cells Technology Research Center, Shiraz University of Medical Sciences, Shiraz, Iran

⁴Clinical Neurology Research Center, Shiraz University of Medical Sciences, Shiraz, Iran

⁵Shiraz Nephro-Urology Research Center, Shiraz University of Medical Sciences, Shiraz, Iran

ABSTRACT

Background: Liver transplantation is the gold standard treatment for end-stage liver failure, but the scarcity of organ donors is the main limiting factor for performing liver transplant surgery.

Objective: The objective was to evaluate hepatocytes' phenotype and functionalities after co-culturing with endothelial (HUVEC) and stellate cells (LX2) in the decellularized liver.

Methods: The livers were decellularized with 1% sodium lauryl ester sulfate (SLES). Cell removal and preservation of extracellular matrix (ECM) ultrastructure were studied by staining, scanning electron, and Raman confocal microscopy. The cell viability was evaluated by MTT, and the functions of cells were assessed on a decellularized scaffold with/without co-culturing with HUVEC and LX2 cell lines. The results were then compared to cells with the same condition on collagen scaffolds.

Results: The data confirmed that SLES prevented the destruction of the liver ECM ultrastructure along with nuclear material removal. Raman spectra confirmed DNA and cell debris removal. The decellularized liver was suitable for cell survival, but the proliferation rate was lower than those cultured in collagen. The tests showed that the function of individual cells on the decellularized scaffold was better than that in collagen scaffolds. Co-culturing with HUVEC and LX2 cell lines did not improve hepatocyte functions.

Conclusion: As a biocompatible scaffold, co-culturing hepatocytes with endothelial and stellate cells within the decellularized liver improved liver-specific functions.

KEYWORDS: Liver; Organoid; Decellularization; Collagen; Hepatocyte; Scaffold

INTRODUCTION

The liver is the largest organ in the human body, with a complex structure and various vital functions [1]. Liver

malfunction is the etiology of many diseases, sometimes leading to mortality. Over 500 million people worldwide suffer from chronic liver disease, which accounts for 2% of the total mortality rate. The global number of deaths from cirrhosis increased, but age-standardized death rates (ASDRs) declined. However, the ASDR for cirrhosis increased over this period. The number of deaths from cirrhosis is projected to increase in the next decade [2, 3].

Today, liver transplantation is the gold standard treatment for end-stage liver failure.

*Correspondence:

Zahra Vojdani, PhD & Zahra khodabandeh PhD
Laboratory for Stem Cell Research, Department of Anatomy,
School of Medicine, Shiraz University of Medical Sciences,
Shiraz, Iran
Stem Cells Technology Research Center, Khalili Avenue,
Shiraz, Iran

ORCID: 0000-0001-8214-2309 & 0000-0003-2276-2674

Tel/Fax: +98-713-2304372 & +98-713-6281563

E-mail: vojdaniz@sums.ac.ir & zahrabandeh@gmail.com

Still, the scarcity of organ donors is the main limiting factor for performing liver transplant surgery [4], and the growing incidence of hepatitis C and fatty liver reduces the number of eligible donors even further [5, 6]. On the other hand, increasing pressures for drug discovery regulations, along with economic and practical reasons, lead to the development of novel and effective therapeutic methods, which also carry certain side effects in humans due to their chemical synthetic nature [7]. Also, variations in human and animal biology render most animal-based tests impractical [8, 9]. All the mentioned issues call for urgent substitute strategies to overcome the existing limitations.

Today, with many sales and companies worldwide, tissue engineering is a progressive field that offers innovative technologies to facilitate the reconstitution of vital organs and overcome existing barriers such as organ shortage and end-stage organ failure [10, 11]. Regenerative medicine uses cells, scaffolds, growth factors, other signaling molecules, and/or genetic manipulation to restore, regenerate, or replace cells, tissues, or organs in vivo and in vitro by restoring normal function through endogenous healing. It is an established field of medicine. Tissue engineering lies at the intersection of regenerative medicine and biomedical engineering [12]. Together, these fields focus on providing care for complex, chronic diseases rather than treatments to manage the disease [13, 14]. More recently, scientists have begun to recognize the importance of the extracellular matrix (ECM) in tissue formation and development, and thus, a potential for use in tissue engineering and regenerative medicine. In this regard, decellularized ECM (dECM) has the ability to stimulate a remodeling and repair response in vivo by inducing an M2 macrophage phenotype rather than an M1 macrophage response during inflammation and fibrosis [15, 16]. Researchers have also found that dECM can promote a more stable cell phenotype [17].

Liver regenerative medicine encompasses an array of diverse methods, including cell therapy, immunomodulation therapy, and liver

tissue engineering, which are intended to replace or reconstruct the liver or restore the function of failing hepatocytes. Remarkable achievements in liver tissue engineering have provided new opportunities for studying complex physiological and pathological processes in vitro [8].

Developing three-dimensional (3D) liver organoids is one great accomplishment that has attracted much attention over the last ten years. Organoids are small, simple versions of real organs created in vitro by inserting the tissue-specific cells in an ECM [18]. The source of cells is from a wide range, including primary adult cells, stem cells, inducible pluripotent stem cells, embryonic stem cells, and cell lines [9, 18]. Liver organoids have great potential for tissue engineering [18]; also, they can be used as a good tool for disease modeling [19, 20], pre-clinical drug screening [7, 21, 22], and personalized medicine [23].

The liver organoids have been shown to be successfully cultured on ECM derived from decellularized tissue [5], matrigel, and synthetic or biological hydrogels [18]. Over the last decade, numerous studies have shown the suitability of applying natural ECM scaffolds derived from decellularized human or animal tissues in regenerative medicine and tissue engineering strategies [24, 25]. Decellularized organ-specific ECM is also a bioink tool for 3D bioprinting construction [26-28]. Besides, it would be a useful in vitro model for exploring its potential roles due to its capabilities in maintaining a nearly intact ultrastructural architecture and composition [29]. So far, decellularization techniques have been used successfully for some organs such as the heart [30], kidney [31, 32], skeletal muscle [33], lung [34], liver [35], gastrointestinal tract [36], testis [37], and ovary [38].

Liver ECM plays a key role by providing a framework for liver cells to facilitate cellular attachment, migration, and control of differentiation, repair, and cell growth [24, 39]. In addition, it forms an ideal microenvironment for the hepatocytes to sustain their phenotype and functionality [4]. An appropriate cell culture

system that can reflect a basic in vivo environment meets the prerequisites. It maintains the liver-specific functions of hepatocytes because liver cells quickly lose their original growth conditions during cell isolation [40].

There is compelling empirical evidence that decellularization-recellularization technology provides a valuable platform for liver bioengineering through the reconstruction of the ECM scaffold of the liver with its parenchymal and non-parenchymal cells, which is at least part of the complexity of the natural texture. Therefore, the current study aimed to evaluate the hepatocytes' phenotype and functionalities when co-culturing with the endothelial and stellate cells in the decellularized liver scaffold.

MATERIALS AND METHODS

Collagen Isolation and Scaffold Fabrication

As previously reported, collagen type I was extracted from the rat tail tendon and treated with 0.02 M acetic acid [41]. We initially lyophilized the collagen solution overnight by freeze-drying (Christ Alpha 2-4 LD-plus, Osterode am Harz, Germany) to generate the scaffolds to obtain collagen powder. Next, 10 mg/mL of the collagen powder was dissolved in 0.5 M acetic acid (1% w/v) on ice, and 1 mL of the mixture was poured into a well of a 24-well plate culture dish (Jetbiofil, China). The plate was kept at -80°C overnight and subsequently frozen-dried to form a collagen sponge [42].

Decellularized Liver Scaffold Preparation

Healthy mice (10-12 weeks old) were sacrificed to obtain liver for decellularization. To prepare the decellularized scaffold, we first removed the livers from the bodies of adult mice, and then they were washed with distilled water and immersed in phosphate buffer saline (PBS) for 30 min. The samples were then placed in distilled water for 16-18 h at 25°C on a magnetic stirrer at 200 RPM to allow the removal of the blood in the liver sample completely. After that, the specimens were decellularized with 1% Sodium Lauryl Ester Sulfate (SLES, Kimia

Sanaat Ataman Co., Tehran, Iran) for 16-18 h at room temperature on a magnetic stirrer at 200 RPM. Next, the samples were placed in a 1% Triton X100 for 30 min. At the next stage, the specimens were rinsed several times in PBS to remove the cell remnants and traces of chemical reagents. Decellularized tissues were fixed in 10% neutral-buffered formalin and 2.5% glutaraldehyde, kept at -80°C, and freeze-dried until further use.

Chemical Crosslinking

Collagen sponges and freeze-dried decellularized livers were chemically crosslinked within a sterile solution of 50 mM 2-N-morpholino ethanesulfonic (Sigma, USA) in 70% ethanol (pH 5.4) containing 5mM 1-ethyl-3-[3dimethylaminopropyl] carbodimide (Sigma, USA) and 2 mM of N-hydroxysulfosuccinimide (NHS, Sigma, USA) for 4 h at 37°C.

This solution was then removed, and the scaffolds were treated with 0.1 M Na₂HPO₄ for 30 min to inhibit the crosslinking reaction. To prepare the samples for cell culture, we rinsed the scaffolds several times with sterile double distilled water, and the crosslinked scaffolds were frozen at -80°C and freeze-dried; then, they were sterilized by 70% ethanol and finally washed several times with sterile PBS.

Raman Confocal Microscopy

To find DNA and cell debris depletion, we prepared decellularized and intact samples for Raman confocal microscopy. The samples were lyophilized (Christ, Alpha 1-2 LD, Germany), and a powder was prepared. A laser at a wavelength of 633 nm was used, and the Raman spectra were analyzed in the range of 500 to 2500 cm⁻¹.

Culture of HepG2, HUVECs and LX2

Hepatoblastoma (HepG2), human umbilical vein endothelial cells (HUVECs), and stellate cells (LX2) (purchased from Pasture Institute, Iran) were cultured in the complete Dulbecco's Modified Eagle's Medium/F12 (DMEM/F12) medium (Bio idea, Iran) supplemented with 10% FBS, 100 U/mL penicillin, and 100 µg/mL streptomycin and incubated at 37°C in 5% CO₂ to reach confluence. HepG2 alone at a

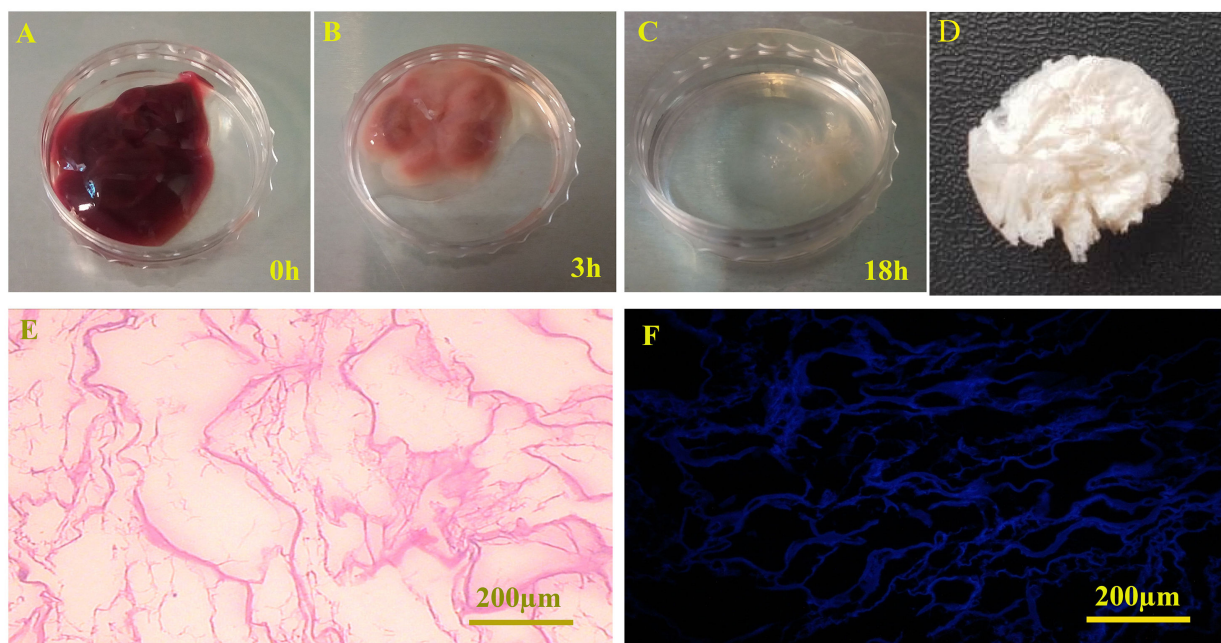


Figure 1: Chronological macroscopic and microscopic changes of the mice liver during the SLES-based decellularization process. (A-C) The color of the liver samples turned from red to white, while the samples preserved their shape and homogeneity, (D) A lyophilized decellularized scaffold with visible pores, (E) Hematoxylin and eosin, and (F) Hoechst staining of the decellularized liver showed it was devoid of nucleic materials.

density of 4×10^5 cells was loaded per well of a 96-well plate or co-cultured with 1×10^5 HUVEC and 5×10^4 LX2 cell lines per well for 7 days.

Experimental Design

To evaluate the effects of decellularized scaffold

and co-culturing on hepatocyte functions, four groups were considered including group 1 (Collagen+HepG2), group 2 (Decellularized liver+HepG2), group 3 (Collagen scaffolds were loaded with HepG2, HUVECs, and LX2 cells) and group 4 (Decellularized livers scaffolds were loaded with HepG2, HUVECs, and LX2 cells).

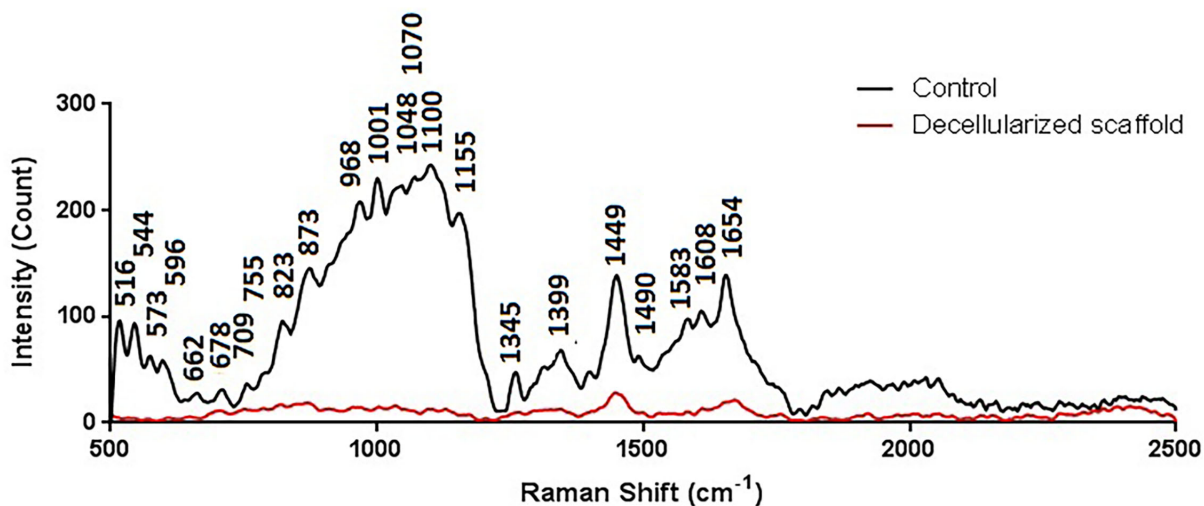


Figure 2: Raman confocal microscopy showed DNA and cell debris depletion after decellularization.

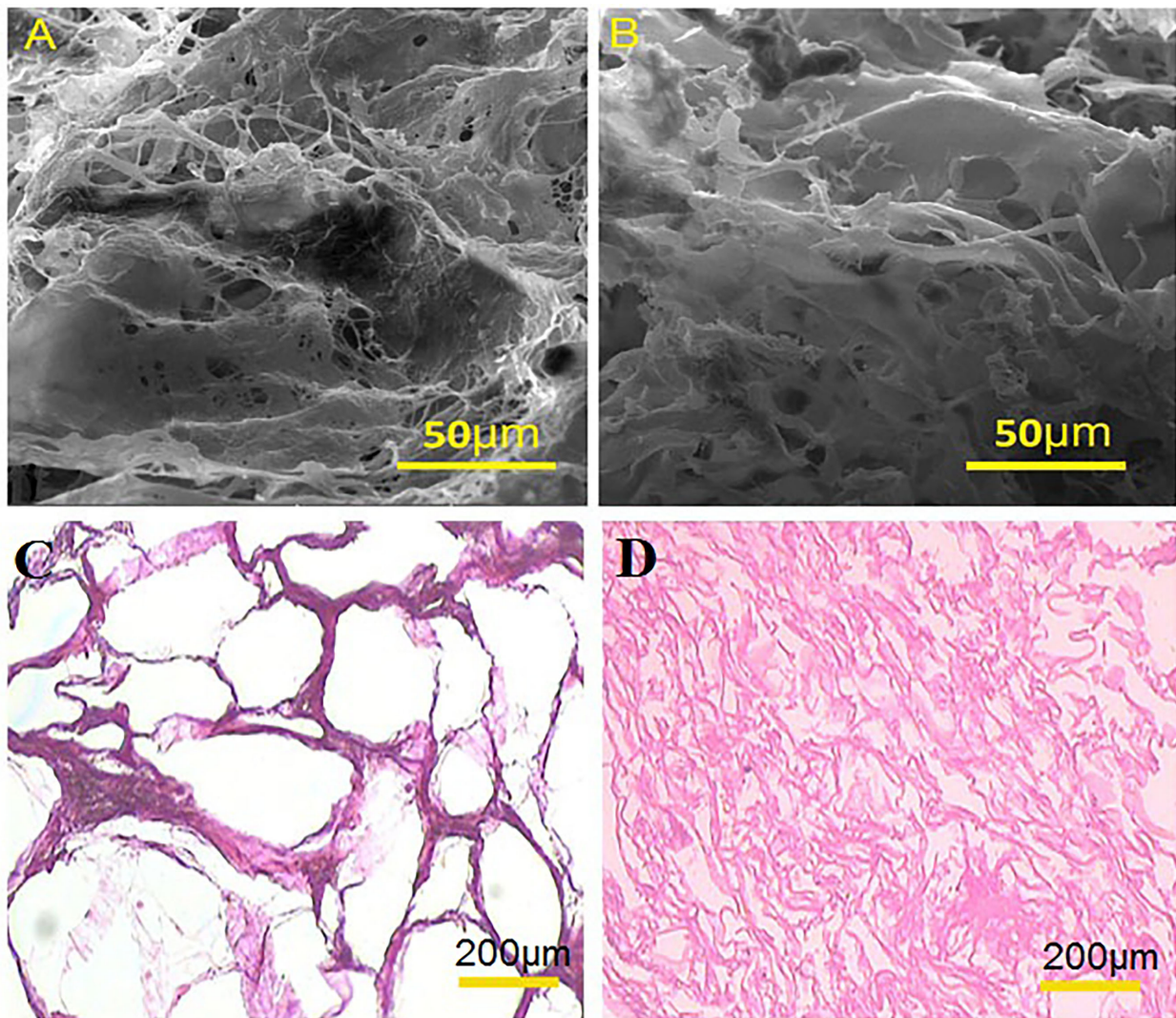


Figure 3: Scanning electron microphotographs and light microscopy of decellularized liver and collagen scaffolds. (A) SEM image of decellularized liver scaffolds showed the efficient removal of cells and good preservation of three-dimensional structures and integrity after decellularization, (B) SEM microphotograph of three-dimensional collagen scaffold with interconnected pores, (C) Light microscopy of the decellularized liver scaffolds, and (D) Collagen scaffold stained with H&E shows a complex network of fibers and collagen bundles with well-defined integrity.

Histological Evaluation and Scanning Electron Microscopy

To study the histology and ultrastructure of the scaffolds, we loaded the collagen or decellularized liver scaffolds with either HepG2 or co-culturing of the same number of HepG2 cells with HUVEC and LX2 cells, as described in the experimental design section.

For ultrastructural assessment, the cell-seeded and cell-free scaffolds were fixed with 2.5% glutaraldehyde, and then, the samples were

dried in a freeze-dryer. In the next step, the samples were coated with a thin layer of gold using a Q150R-ES sputter coater (Quorum Technologies, London, UK) and imaged using a VEGA3 microscope (TESCAN, Brno, Czech Republic) at 10 kV accelerating voltage.

The cell-seeded and decellularized scaffolds were fixed with 10% neutral buffered formalin (pH 7.4) and embedded in paraffin for histological assessments. The paraffinized blocks were sectioned at 5–10 μm thickness; the sections were stained with hematoxylin and

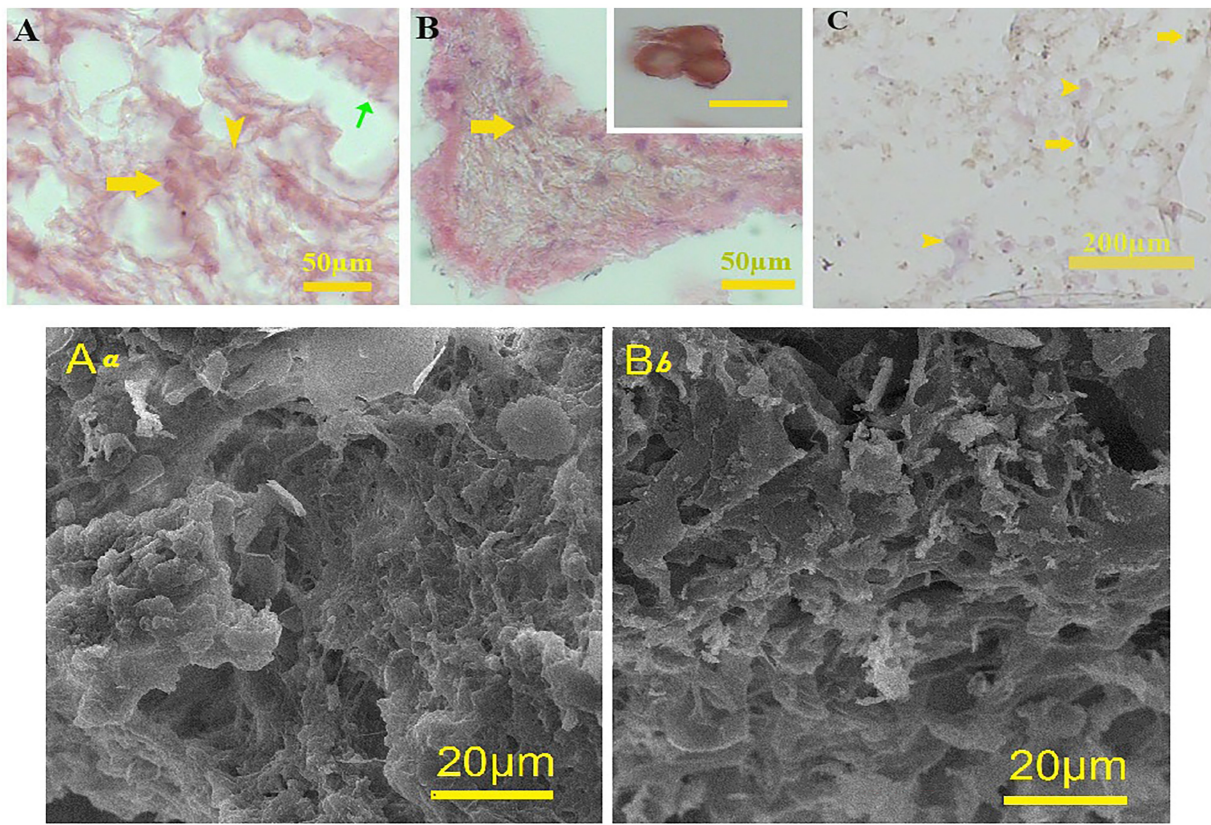


Figure 4: The three types of cells were loaded on the decellularized liver. **(A)** HepG2 cells (yellow arrow), detected by the glucose 6-phosphatase activity test, are brown in color. In addition, the cytoplasm of other types co-cultured with HepG2 was stained with eosin (arrowhead). The cells with elongated nuclei surrounding luminal structures seem to be endothelial cells (green arrow), **(B)** The cells within the collagenous part of the scaffolds show a fibroblast-like structure, which may represent the stellate cells (yellow arrow). The small square showed some glucose 6-phosphatase-positive cells, HepG2, and **(C)** Glucose 6-phosphatase-positive cells (arrows) along with the other cell types (arrowheads) in the collagen scaffold. **(Aa)** SEM microphotographs show that the cells are distributed on the decellularized liver and **(Bb)** Collagen scaffolds.

eosin (H&E) and Hoechst (Sigma-Aldrich) and examined by light (Olympus BX61, Tokyo, Japan) or fluorescent (Olympus, BX51, Japan) microscopes equipped with a digital camera (Olympus DP73), respectively.

MTT Assay

The cell viability and proliferation capacity were evaluated using 3-(4,5-dimethylthiazol-2-yl)-2, 5-diphenyl tetrazolium bromide (MTT, Sigma) assay. The cells were seeded at a density of 1×10^4 /well of a 96-well plate for 1, 3, and 5 days. The culture media were then replaced by 1 mg/mL of MTT in DMEM and incubated at 37°C in 5% CO₂ in a dark environment for 3h. The dye was then eluted with-

Dimethyl sulfoxide, and optical density was measured at 595 nm.

Attachment Assessment

HepG2 cell lines at a density of 2×10^5 cells were seeded on either collagen or decellularized scaffolds for 1 h. Then, the medium was removed, the number of unattached cells was counted by hemocytometer slides, and the final number was subtracted from the initial cell count.

Liver Functional Assessments

Indocyanine Green Clearance Assay

The culture media were replaced by 1 mg/mL of indocyanine green (ICG) (Sigma, USA) in DMEM for 15 minutes. Subsequently, the ICG solution was removed, and the ordinary

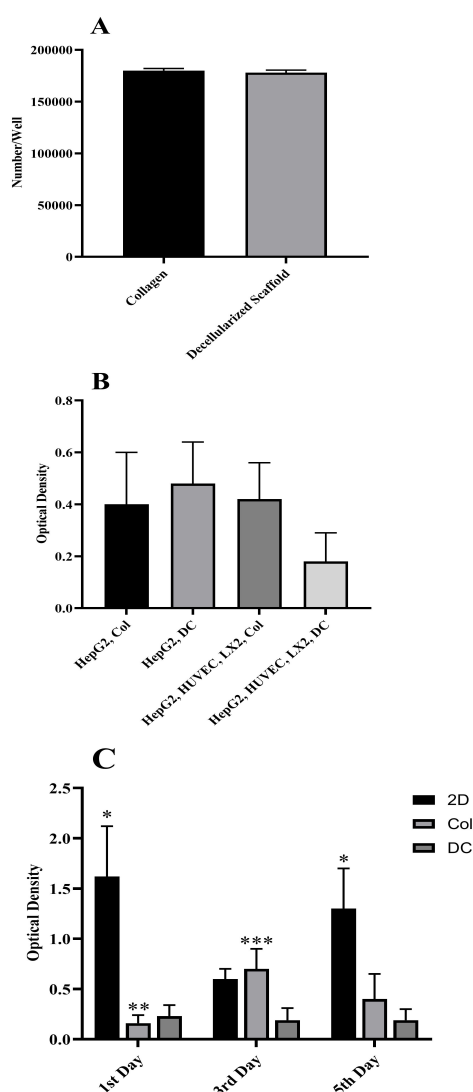


Figure 5: Evaluation of the cell attachment, viability, and function to decellularized liver and collagen scaffolds. (A) The statistical analysis showed no significant difference in the adhesion of HepG2 cells on the two scaffolds, (B) The comparison of the MTT test of the HepG2 cultured on the decellularized liver and collagen scaffolds with those cultured in two-dimensional conditions, and (C) Comparison of the optical density of the uptake and release of the ICG in decellularized liver and collagen scaffolds. There is no significant difference between the groups.

*Significant differences with the collagen and decellularized liver scaffolds of the same day and two-dimensional culture on the third day after culture ($P < 0.05$).

**Significant difference with the cells cultured on the same scaffold on the third day ($P < 0.05$).

***Significant difference with the cells cultured on the decellularized liver scaffold on the same day ($P < 0.05$).

culture media were replaced for the next 3 h. The uptake and release of the dye were evaluated by assessing the optical density of the media at 820 nm. Cell-free scaffolds were used as blank.

Glucose 6-Phosphatase Activity Assay

At first, HepG2 cells, at a density of 4×10^6 cells per well of a 24-well plate, or the same cell number of HepG2 with 1×10^6 HUVECs and 5×10^5 LX2 cells per well, were seeded on the collagen or decellularized scaffolds. After 7 days, the unfixed samples were embedded in an OCT compound (Optic Planet Tissue Tek). The OCT blocks were sectioned using a cryostat (Leica CM1850, Germany) at a thickness of $15 \mu\text{m}$ and then collected on gelatin-coating microscope slides. Then, the fresh unfixed cryostat sections were placed into an incubating medium containing 0.125% glucose 6-phosphate (Sigma-Aldrich) and 2% lead nitrate (Merck) in tris maleate buffer at pH 6.7 at 37°C for 5–20 min. Then, the sections were washed twice for 2 min each in distilled water. In the next step, the samples were immersed in 1% ammonium sulfide and washed in distilled water. The sections were fixed in 10% formaldehyde for 15–30 min, rinsed with distilled water, and mounted. The intensity of the reaction was scored according to an arbitrary scoring system.

Glycogen Detection Assay

We evaluated the glycogen storage capability by the hepatocytes; the frozen sections were immersed in 1% periodic acid for 5 min and then incubated in Schiff reagent for 15 min. Then, the sections were dehydrated in increasing grades of ethanol, cleared on xylon, and mounted. The intensity of the reaction was scored according to an arbitrary scoring system.

Urea Production Assay

The urea level of the culture medium was determined using a quantitative detection kit of the Urea UV (Pars Azmoon), according to the manufacturer's instructions. The principle of this test is based on the enzymatic activity of Urease-Glutamate dehydrogenase.

Ethical Considerations

All stages of animal study, including anesthesia, surgery, animal care, and euthanasia, were performed according to the ethics committee guidelines of Shiraz University of Medical Sciences (IR.SUMS.REC.1395.S1173).

Statistical Analysis

The analysis of variance (ANOVA) was used to analyze the data. Post-hoc analyses were performed by Tukey and LSD test. The data were analyzed using SPSS software 25.0 for Windows. The graphs were depicted by GraphPad Prism ver 9.0 software. A p-value of <0.05 was considered as significant. All experiments were performed in triplicate.

RESULTS

Decellularized Scaffold Assessments

During the mice liver decellularization process, the liver color changed from red to white and became semi-transparent. The samples retained their shape and integrity during the process, and after the lyophilizing decellularized liver, the pores of the scaffolds were preserved (Fig. 1A-1D, respectively). Both H&E and Hoechst staining showed that the scaffolds were devoid of nucleic materials (Fig. 1E, 1F).

Raman Confocal Microscopy Results

We performed Raman confocal microscopy to characterize the decellularized tissue and find the DNA depletion. DNA removal was confirmed after the decellularization process. The peak at 678 cm⁻¹ is assigned for ring breathing modes in the DNA bases. Also, the peak at 1070-1090 cm⁻¹ represents symmetric PO₂ stretching of DNA (represents more DNA in the cell) [43]. Vibration at 1345 cm⁻¹ represents α -helical proteins and deoxy adenosine [44]. A peak at 1490 cm⁻¹ was assigned to DNA as well. Cytosine and guanine Raman spectra are at 573 and 1608 cm⁻¹ [43]. A decrease in the Raman intensity shows DNA depletion after decellularization.

A peak at 544 cm⁻¹ represents bending in the α -glycosidic bond in sugar such as glucose

[45], and at 1048 and 1155 cm⁻¹ is assigned to glycogen. Glycogen is the main storage particle in hepatocytes. After decellularization, nearly all glycogen is washed out. This also confirms the efficiency of the decellularization protocol.

A peak at 596 cm⁻¹ represents phosphatidylinositol present in the cell membrane. Also, 668 and 1070 cm⁻¹ bonds are assigned to lipid and triglyceride (fatty acid). A peak at 1100 cm⁻¹ represents the C-C vibration mode [43]. CH₂ stretching mode and C-H vibration in protein and lipids were also assigned to 1399 and 1449 cm⁻¹ [43, 46, 47]. Lipids and phospholipids are the most important components of cell membranes. They also showed a significant decline after decellularization, which indicated cell debris removal.

Peaks at 755, 823, 873, and 1000 cm⁻¹ were assigned to symmetric breathing of tryptophan and tyrosine, hydroxyproline, and phenylalanine, respectively (protein assignment). Besides, a peak at 1583 cm⁻¹ was assigned to the C-C bending mode of phenylalanine [43]. In the liver, most of the protein composition exists in the cytoplasm of the hepatocytes. The decline in the protein content indicated cell lyses as well. The liver is a cell-rich tissue with a low amount of ECM.

The peaks at 662 cm⁻¹ were assigned to the C-S stretching mode of cystine; at 873, they were assigned to hydroxyproline; at 1554 cm⁻¹, they represented Amide I (collagen type I). Although histological sections showed the presence of collagen fibers in ECM, Raman confocal microscopy revealed extensive washing out of collagen by the decellularization process (Fig. 2).

Histological and SEM Assessments

SEM assessment showed that the integrity of the microarchitecture was preserved well, and the cells were removed with high efficiency after decellularization. The SEM image of the decellularized liver scaffolds represented a complex network of fibers with porous structures once filled with cells. Moreover, the investigation of the shape and structure of the

decellularized liver and the collagen scaffolds by light microscope showed a complex network of fibers with good integrity (Fig. 3).

Cell Morphology Assessments

The cell morphology was studied on collagen and decellularized liver scaffold by H&E staining. In this staining, HepG2 cells were well distributed and bound to collagen strands in both collagen and decellularized liver scaffolds. However, the number of cells in the collagen scaffold seemed much higher (data was not shown).

In the other experiment set, the HepG2 cell lines were detected by assessment of glucose 6-phosphatase activity along with H&E staining of HUVEC and LX2 cell lines. In these sections, the HepG2 cells were stained brown, and it was revealed that the hepatocytes, along with other cell types, could be alive in different scaffolds (Fig. 4A-4C). In addition, SEM revealed the cells expanded on both scaffolds properly (Fig. 4Aa, 4Bb).

Attachment Evaluation

The cell attachment assay showed that $89.08\% \pm 3.95\%$ of the cells were attached to the decellularized liver scaffold, and $90.89\% \pm 3.253\%$ were attached to the collagen scaffolds. The adhesion property of the two types of scaffolds was statistically similar ($P < 0.05$) (Fig. 5A).

Cell Viability Assay

To determine the cytocompatibility of decellularized scaffolds, the viability and proliferation of HepG2 on decellularized liver and collagen scaffolds were assessed and compared with two-dimensional (2D) culture conditions. On the first day, the cell viability in the 2D culture condition was significantly higher than the other groups in the three-dimensional cultures on the same day ($P < 0.0001$). On the third day, the number of viable cells on the collagen scaffolds significantly increased compared with those on the corresponding cultures on the first day ($P = 0.014$). On the fifth day, the highest number of viable cells presented on the 2D culture condition ($P < 0.0001$). Also, on the third day, the number of viable cells

on the collagen scaffolds showed a significant increase compared to those cultured on the decellularized scaffold ($P = 0.027$). MTT test showed that the seeded HepG2 on the decellularized scaffolds were viable, and the number of live cells on this scaffold was equal statistically to those on collagen scaffold at day 5th (Fig. 5B).

Functional Evaluations

The data from ICG analysis showed that the cell cultures on both decellularized liver and collagen scaffolds could be functional, and the HepG2 on decellularized liver showed insignificantly higher releasing amounts of the dye. The data showed that the release of indocyanine green from the HepG2 cells was similar in all conditions, regardless of the type of scaffolds or co-culturing system (Fig. 5C).

The brown color in the light microscope images reflects the glucose 6-phosphatase activity. According to an arbitrary scoring system, a vigorous color intensity was observed in decellularized liver scaffolds containing HepG2 compared to that on the collagen scaffold, and the cultures contained three types of cells on decellularized liver scaffolds. This suggests that a decellularized liver scaffold is a more suitable substrate for glucose 6-phosphatase activity by HepG2 cells. Still, co-culturing of the cells did not positively increase the activity of this enzyme in both scaffolds (Fig. 6).

Although the ability to produce and store glycogen was observed in all culture conditions, HepG2 in decellularized liver scaffolds showed a "higher" color intensity than the other conditions. HepG2 cells in the collagen scaffold, with a much larger number of cells, stored a lower amount of glycogen, and the co-culture systems in both decellularized and collagen scaffolds showed "moderate" staining intensity (Fig. 7).

After 7 days of cell culture, HepG2 cells produced a statistically similar amount of urea in all culture conditions (Fig. 8).

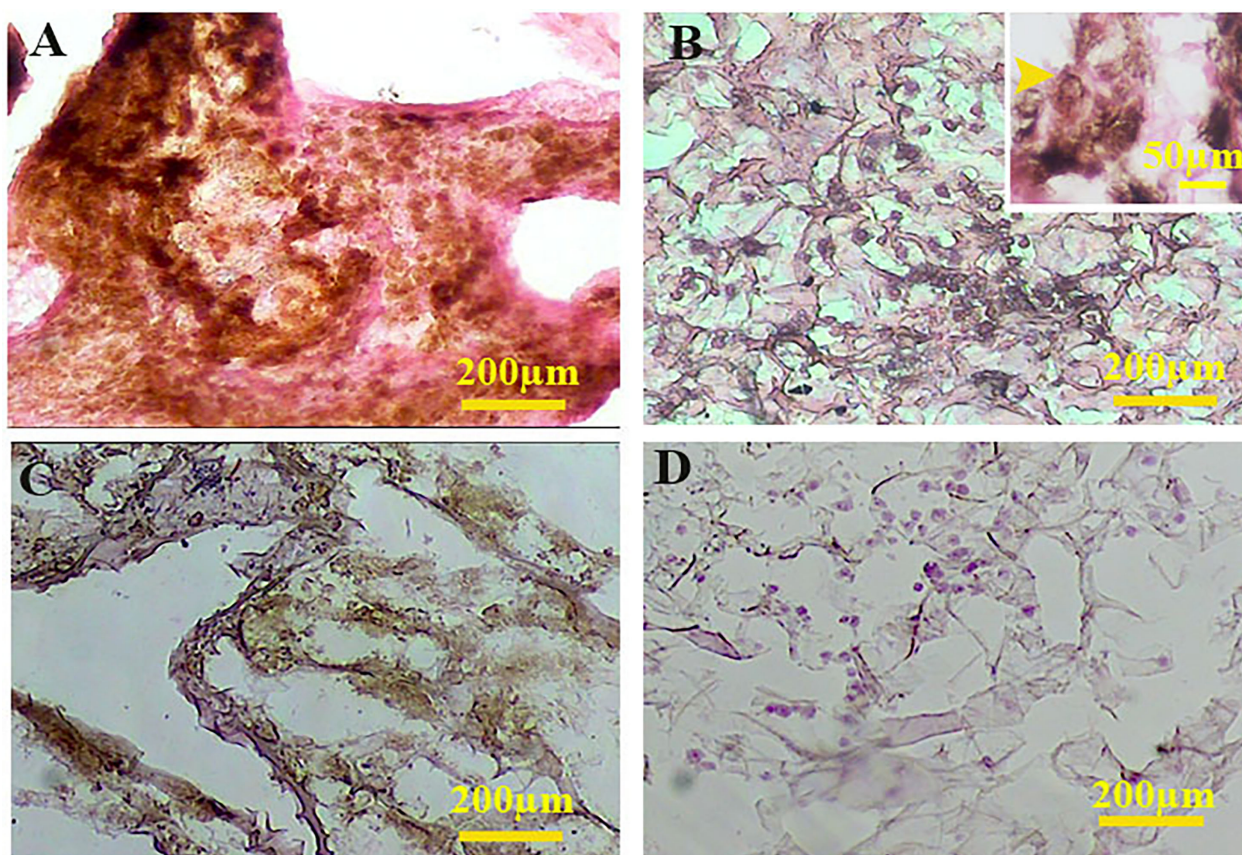


Figure 6: Comparison of the glucose-6 phosphatase activity by HepG2 cells in each culture condition. (A) The HepG2 cells in the decellularized liver scaffolds show the "highest" staining intensity, (B) The HepG2 cells in the collagen scaffold show "moderate" enzyme activity, (C) The enzyme activity in HepG2 in the co-culture condition on the decellularized scaffold showed a "moderate" intensity, and (D) The enzyme activity of the HepG2 cells in the co-culturing system with HUVEC and LX2 cell lines on the collagen scaffold shows "weak" intensity.

DISCUSSION

In the first step of liver organoid fabrication, a scaffold from the decellularized mice liver using SLES was prepared, demonstrating the ability to recellularize and boost some hepatocyte functions in vitro. It has been reported that the cells in a 3D condition revealed higher levels of desirable physiological functions, including survival, morphology, proliferation, differentiation, response to stimulation, migration, angiogenesis, drug metabolism, gene expression, protein synthesis, and cellular function [48]. The liver ECM constitutions provide the liver cells with a framework that facilitates cell functions, tissue growth, and repair [19, 49, 50]. Due to its chemical composition, biophysical properties, and interaction with the cultured liver cells, the ECM framework also af-

fects the expression of liver-specific genes and cellular responses to the peripheral signals [7, 8]; it creates an optimal microenvironment in which the liver cells' phenotype and function are maintained [4]. Our data also indicated a higher hepatocyte function in the decellularized scaffold.

Devising a standard protocol to sustain the chemical nature and architecture of a cell-free ECM was one of the goals of the present study. Even though SDS is a routine substance in many decellularization protocols, its considerable degradation effects on essential ligands and ECM proteins have resulted in the use of mild detergents such as SLES and other anionic detergents such as Triton X100 [4, 51, 52], which maintain the ECM structure and composition [51, 52]. Our SEM, H&E, and Hoechst data confirmed that SLES prevented

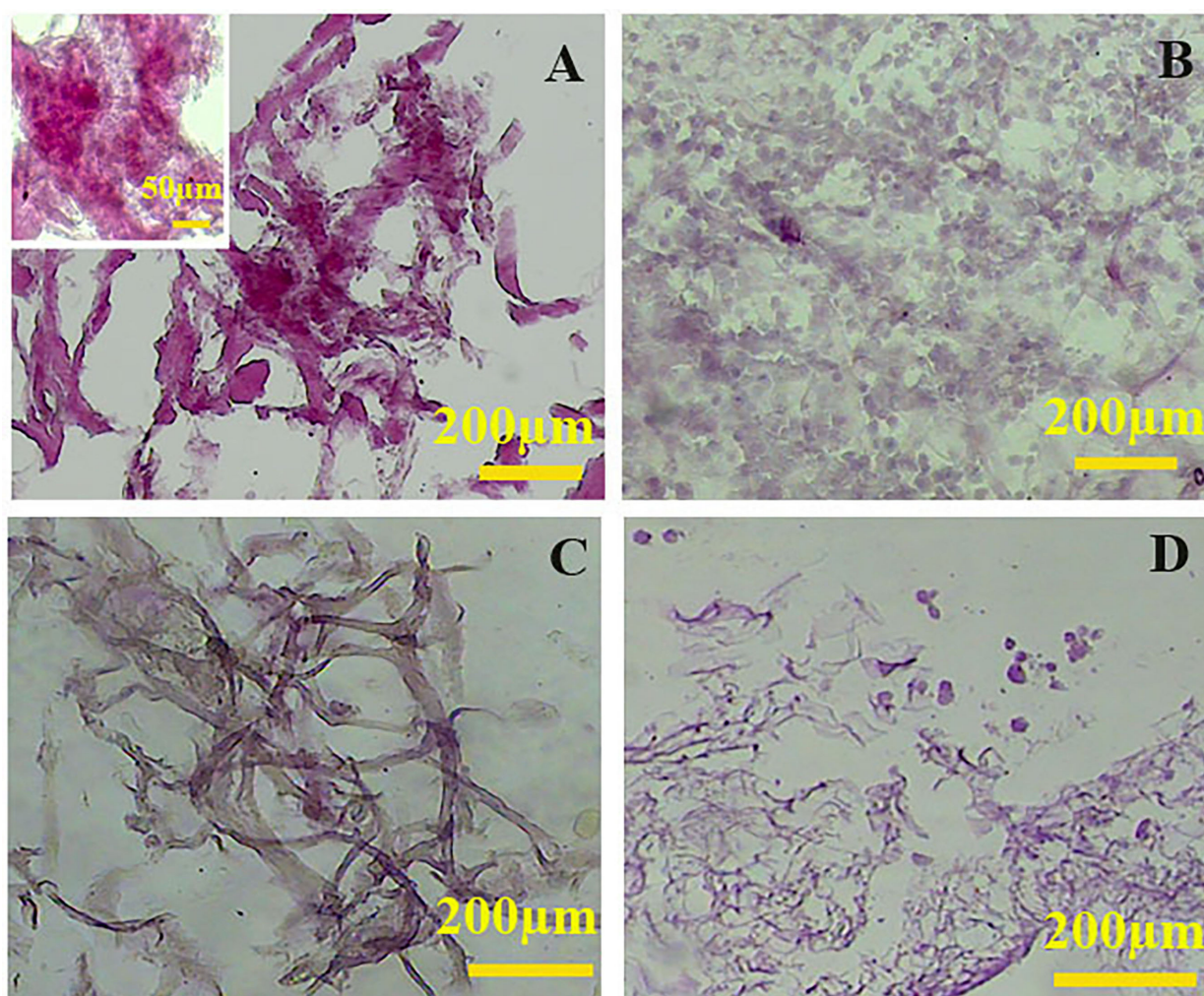


Figure 7: Comparison of the amount of glycogen production and storage by HepG2 cultured in various conditions. The purple and dark red color indicates the glycogen accumulation in the HepG2 cytoplasm. (A) The HepG2 cells cultured on the decellularized liver scaffolds show the "highest" PAS reaction intensity compared with the other conditions. (B) HepG2 cells cultured on the collagen scaffold exhibit "weaker" intensity, (C) The HepG2 cells show a "moderate" intensity of the reaction of glycogen when they cultures on the decellularized scaffold along with HUVEC and LX2 cell lines, and (D) HepG2 cells cultured on collagen scaffold with other cell types show a "moderate" staining intensity.

the removal of both the liver ECM ultrastructure along nuclear material removal.

Biocompatibility of the decellularized scaffolds is another concerning issue, as the cellular debris and detergent trace inside the scaffold may cause cell damage during the cell culture. In our study, HepG2 remained alive on the decellularized liver scaffolds. The cell viability index on this scaffold was statistically similar over time, and functional tests, SEM, and light microscopy showed that decellularized liver scaffolds were non-toxic and compatible

with cell survival and functions. In addition, it was observed that despite the increased activity of proper cells, the proliferation rate decreased compared to those cultured in the collagen scaffolds. This might be because they were located in a microenvironment similar to their intact niche. In the intact niche, hepatocyte proliferation is limited, while cell division increases after tissue damage; therefore, it is likely that this environment can restrict cell proliferation in the same way as in the physiological niche inside the body.

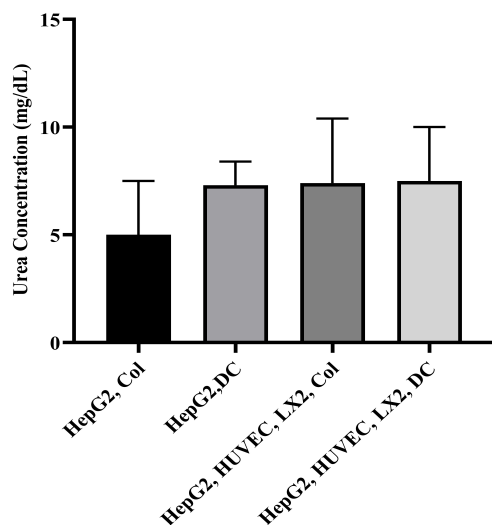


Figure 8: The total amount of urea production by HepG2 cells in various conditions

It has also been reported in former studies that ECM's 3D scaffold can serve as an ideal environment that supports the growth and function of various liver cell types [53, 54]. Evidence indicates that the utilization of ECM as a bioink in 3D printing develops a scaffold on which the hepatocyte can survive and function [55]. Following that, Mazza *et al.*, suggested that the decellularized liver scaffold could be an essential step forward in making artificial liver [56].

Lower viable cell numbers on decellularized scaffolds may be attributable to fewer primary cell attachments on the decellularized scaffold. To test the hypothesis, the HepG2 cell attachment to decellularized and collagen scaffolds was assessed, which revealed that cell attachment on both scaffolds was about 90% with no significant statistical difference. The cell attachment and MTT assay data indicated that cell proliferation on the decellularized liver scaffold was less than on the collagen scaffold. Still, the cell function improved in the decellularized liver environment. Previous studies have also shown that cells can adhere to 2D and 3D decellularized liver scaffolds [57]. Also, light microscopy images in this study showed that all three types of cells, *i.e.*, HepG2, HUVECs, and LX2, could grow on the decellularized liver scaffolds.

Although microscopic images and MTT assay revealed higher numbers of cells on the collagen scaffold, the results of functional tests such as glycogen storage and glucose 6-phosphatase activity showed that the performance of each HepG2 cell on a decellularized liver scaffold was better than its function on the collagen scaffolding as indicated by the intensity of the reaction for each cell. Also, based on these data, the activity of HepG2 cells alone on decellularized liver scaffolds was higher than when co-cultured with HUVECs and LX2. According to previous studies, the hepatocytes differentiated from human embryonic and induced pluripotent stem cells on a 3D scaffold of the mouse decellularized liver showed higher lipid synthesis, glycogen production, albumin expression as an adult hepatocytic marker, and a reduction in Alpha-fetoprotein (AFP) expression, as a marker of embryonic hepatocytes, compared with that differentiated in the 2D culture system [58]. In another study, human umbilical mesenchymal stem cells were induced to differentiate on the decellularized liver (3D), and the functions of newly differentiated hepatocytes were compared with those on the monolayer culture (2D), monolayer on the decellularized liver (2D), and cell aggregate (3D) conditions. They showed that the cells on the 3D decellularized liver scaffold produced higher levels of albumin, CK-18, glycogen storage, and ammonia conversion to urea. In addition, decellularized liver scaffolds also impact the differentiation competence of the umbilical-derived stem cells into hepatocytes and their phenotype improvement [59]. The results of this study confirmed the previous studies and showed that glycogen storage by each cell on the decellularized liver scaffolds was higher.

The current study findings revealed that the urea production/uptake and release of indocyanine green were statistically similar in all conditions. These activities depend on the increase in the function of each cell. Since the number of cells in the collagen was more than that in the decellularized liver scaffold, it would be expected that the amount of urea and indocyanine green clearance would be better in the collagen. In contrast, we found that the

data were similar in all conditions. Therefore, it can be concluded that HepG2 cells showed a higher urea production or indocyanine green clearance on the decellularized liver scaffolds than on the collagen scaffold regarding their number. A similar study also showed that urea production was higher in the porcine hepatocyte cultured on the porcine decellularized liver scaffolds than those on the collagen scaffolds [60].

Hepatocytes cultured on porcine liver ECM-derived scaffold have been reported to yield improved functional results for albumin synthesis, urea production, and P450 IA1 activity compared to the collagen type I sandwich or monolayer culture on the collagen type I film [61]. An increase in the production of urea has also been detected by HepG2 cell lines when they have grown on the decellularized rat liver scaffolds [62]. These reports are in line with the results of the present study.

Several reports demonstrated the impact of the co-culturing system on the hepatocytes' function [63-67]. In this study, the hepatocytes alone showed higher function than the co-culturing system on the decellularized liver scaffolds. A hybrid co-culture system was designed to show the influence of an overlaying single layer of the endothelial cells on the embedded HepG2 in a 3D scaffold, and it was revealed that the hepatocyte growth declined in the short term (day 3); however, in the long term, the cell growth increased by paracrine secretions of the endothelial cells, while the liver cell-specific activities, such as albumin secretion and liver-specific gene expression, were significantly increased after 5 days [63]. Contrary to the findings of a previous study, our data showed that the activity of the hepatocytes was not influenced by the co-culturing system after the seventh day. Therefore, it may be concluded that the effect of endothelial cells co-culturing on hepatocyte functions is time-dependent [63]. Modulating inflammatory responses has been reported by co-culturing the hepatocyte with non-parenchymal rat liver cells. In addition, co-culture methods have been suggested as a stable platform for in vitro hepatic models [64]. In another study,

a hybrid co-culturing system of the hepatocytes and endothelial cells was introduced as a valuable system for prolonging the hepatocyte function [65]. It has also been reported that survival and liver function in the co-culture system with 3T3 fibroblast over 18 days was better than that of the hepatocyte culture alone [66].

Further evidence showed the co-culturing of the hepatocytes and hepatic stellate cells facilitated the spheroid formation and affected its structure, suggesting it was a way to maintain some functions of the hepatocytes in the early stages of culture [67]. The results of the two recent studies pointed out the maintenance but not the hepatocyte function improvement for the hepatocyte in the natural niche [66, 67]. In our study, it was also indicated that the functions of hepatocytes were maintained, but not improved, in the co-culture system.

In conclusion, the current study showed that decellularized liver scaffolds based on the SLES improved the function of individual liver cells, including the uptake and release of the indocyanine green, production of the urea, glycogen, and glucose 6-phosphatase activity compared to the collagen scaffolds; however, the proliferation cell rate was higher in the collagen-based scaffolds. The decellularized liver can be considered a potential scaffold for fabricating the liver organoids for different purposes, such as pre-clinical drug screening, disease modeling, and genetic defects.

ACKNOWLEDGMENTS

The authors wish to thank M. Salmannjad, M. Sani, and E. Nadimi for their excellent technical support. The authors would like to thank the Center for Development of Clinical Research of Namazi Hospital and Dr. Nasrin Shokrpour for editorial assistance.

CONFLICT OF INTEREST: None declared.

FINANCIAL SUPPORT: This work was supported by the Vice-Chancellor for Research of Shiraz University of Medical Sciences [Grant no.: 13035] and was performed by L. Talebi as a part of the requirements of the M.Sc. program.

REFERENCES

1. Lee SY, Kim HJ, Choi D. Cell sources, liver support systems and liver tissue engineering: alternatives to liver transplantation. *Int J Stem Cells* 2015;**8**:36-47.
2. Mazza G, Al-Akkad W, Rombouts K, Pinzani M. Liver tissue engineering: From implantable tissue to whole organ engineering. *Hepatol Commun* 2018;**2**:131-41.
3. Huang DQ, Terrault NA, Tacke F, et al. Global epidemiology of cirrhosis - aetiology, trends and predictions. *Nat Rev Gastroenterol Hepatol* 2023;**20**:388-98.
4. Faulk DM, Wildemann JD, Badylak SF. Decellularization and cell seeding of whole liver biologic scaffolds composed of extracellular matrix. *J Clin Experiment Hepatol* 2015;**5**:69-80.
5. Uygun BE, Yarmush ML. Engineered liver for transplantation. *Curr Opin Biotechnol* 2013;**24**:893-9.
6. Bhatia SN, Underhill GH, Zaret KS, Fox IJ. Cell and tissue engineering for liver disease. *Sci Transl Med* 2014;**6**:245sr2.
7. LeCluyse EL, Witek RP, Andersen ME, Powers MJ. Organotypic liver culture models: meeting current challenges in toxicity testing. *Crit Rev Toxicol* 2012;**42**:501-48.
8. Handa K, Matsubara K, Fukumitsu K, et al. Assembly of human organs from stem cells to study liver disease. *Am J Pathol* 2014;**184**:348-57.
9. Yin X, Mead BE, Safaee H, et al. Stem cell organoid engineering. *Cell Stem Cell* 2016;**18**:25-38.
10. Jaklenec A, Stamp A, Deweerd E, et al. Progress in the tissue engineering and stem cell industry "are we there yet?". *Tissue Eng Part B Rev* 2012;**18**:155-66.
11. Langer R, Vacanti J. Advances in tissue engineering. *J Pediatr Surg* 2016;**51**:8-12.
12. Borrelli MR, Hu MS, Longaker MT, Lorenz HP. Tissue engineering and regenerative medicine in craniofacial reconstruction and facial aesthetics. *J Craniofac Surg* 2020;**31**:15-27.
13. McInnes AD, Moser MA, Chen X. Preparation and use of decellularized extracellular matrix for tissue engineering. *J Funct Biomater* 2022;**13**:240.
14. Katari R, Peloso A, Orlando G. Tissue engineering and regenerative medicine: semantic considerations for an evolving paradigm. *Front Bioeng Biotechnol* 2015;**2**:57.
15. Golebiowska AA, Intravaia JT, Sathe VM, et al. Decellularized extracellular matrix biomaterials for regenerative therapies: Advances, challenges and clinical prospects. *Bioact Mater* 2023;**32**:98-123.
16. Kasravi M, Ahmadi A, Babajani A, et al. Immunogenicity of decellularized extracellular matrix scaffolds: a bottleneck in tissue engineering and regenerative medicine. *Biomater Res* 2023;**27**:10.
17. Zhang X, Chen X, Hong H, et al. Decellularized extracellular matrix scaffolds: Recent trends and emerging strategies in tissue engineering. *Bioact Mater* 2022;**10**:15-31.
18. Schneeberger K, Spee B, Costa P, et al. Converging biofabrication and organoid technologies: the next frontier in hepatic and intestinal tissue engineering? *Biofabrication* 2017;**9**:013001.
19. Lancaster MA, Knoblich JA. Organogenesis in a dish: modeling development and disease using organoid technologies. *Science* 2014;**345**:1247125.
20. Underhill GH, Khetani SR. Bioengineered Liver Models for Drug Testing and Cell Differentiation Studies. *Cell Mol Gastroenterol Hepatol* 2018;**5**:426-39.
21. Ramachandran SD, Schirmer K, Müntz B, et al. In vitro generation of functional liver organoid-like structures using adult human cells. *PLoS one* 2015;**10**:e0139345.
22. Ware BR, Khetani SR. Engineered liver platforms for different phases of drug development. *Trends Biotechnol* 2017;**35**:172-83.
23. Nantasanti S, de Bruin A, Rothuizen J, et al. Concise review: organoids are a powerful tool for the study of liver disease and personalized treatment design in humans and animals. *Stem Cells Transl Med* 2016;**5**:325-30.
24. Uygun BE, Yarmush ML, Uygun K. Application of whole-organ tissue engineering in hepatology. *Nat Rev Gastroenterol Hepatol* 2012;**9**:738-44.
25. Crapo PM, Gilbert TW, Badylak SF. An overview of tissue and whole organ decellularization processes. *Biomaterials* 2011;**32**:3233-43.
26. Ji S, Guvendiren M. Recent advances in bioink design for 3D bioprinting of tissues and organs. *Front Bioeng Biotechnol* 2017;**5**:23.
27. Kim BS, Kim H, Gao G, et al. Decellularized extracellular matrix: a step towards the next generation source for bioink manufacturing. *Biofabrication* 2017;**9**:034104.
28. Pati F, Cho D-W. Bioprinting of 3D tissue models using decellularized extracellular matrix bioink. *3D Cell Culture: Springer*; 2017. p. 381-90.
29. Hoshiba T, Chen G, Endo C, et al. Decellularized extracellular matrix as an in vitro model to study the comprehensive roles of the ECM in stem cell differentiation. *Stem cells Int* 2016;**2016**:6397820
30. Hodgson MJ, Knutson CC, Momtahan N, Cook AD.

- Extracellular matrix from whole porcine heart decellularization for cardiac tissue engineering. *Methods Mol Biol* 2018;**1577**:95-102.
31. Destefani AC, Sirtoli GM, Nogueira BV. Advances in the Knowledge about Kidney Decellularization and Repopulation. *Front Bioeng Biotechnol* 2017;**5**:34.
 32. Fedecostante M, Onciu OG, Westphal KG, Maser-euw R. Towards a bioengineered kidney: recellularization strategies for decellularized native kidney scaffolds. *Int J Artif Organs* 2017;**40**:150-8.
 33. Porzionato A, Sfriso MM, Pontini A, et al. Decellularized human skeletal muscle as biologic scaffold for reconstructive surgery. *Int J Mol Sci* 2015;**16**:14808-31.
 34. Skolasinski S, Panoskaltis-Mortari A. Decellularization of Intact Lung Tissue Through Vasculature and Airways Using Negative and Positive Pressure. *Methods Mol Biol* 2018:1577:307-315.
 35. Chen Y, Geerts S, Jaramillo M, Uygun BE. Preparation of Decellularized Liver Scaffolds and Recellularized Liver Grafts. *Methods Mol Biol* 2018;**1577**:255-70.
 36. Nowocin AK, Southgate A, Gabe SM, Ansari T. Biocompatibility and potential of decellularized porcine small intestine to support cellular attachment and growth. *J Tissue Eng Regen Med* 2016;**10**:E23-33.
 37. Kargar-Abarghouei E, Vojdani Z, Hassanpour A, et al. Characterization, recellularization, and transplantation of rat decellularized testis scaffold with bone marrow-derived mesenchymal stem cells. *Stem Cell Res Ther* 2018;**9**:324.
 38. Hassanpour A, Talaei-Khozani T, Kargar-Abarghouei E, et al. Decellularized human ovarian scaffold based on a sodium lauryl ester sulfate (SLES)-treated protocol, as a natural three-dimensional scaffold for construction of bioengineered ovaries. *Stem Cell Res Ther* 2018;**9**:252.
 39. Caralt M, Velasco E, Lanas A, Baptista PM. Liver bioengineering: from the stage of liver decellularized matrix to the multiple cellular actors and bioreactor special effects. *Organogenesis* 2014;**10**:250-9.
 40. Wang G, Zheng Y, Wang Y, et al. Co-culture system of hepatocytes and endothelial cells: two in vitro approaches for enhancing liver-specific functions of hepatocytes. *Cytotechnology* 2018;**70**:1279-90.
 41. Rajan N, Habermehl J, Coté M-F, et al. Preparation of ready-to-use, storable and reconstituted type I collagen from rat tail tendon for tissue engineering applications. *Nat Protoc* 2006;**1**:2753-8.
 42. Rezaei M, Davani F, Alishahi M, Masjedi F. Updates in immunocompatibility of biomaterials: applications for regenerative medicine. *Expert Rev Med Devices* 2022;**19**:353-67.
 43. Movasaghi Z, Rehman S, Rehman IU. Raman spectroscopy of biological tissues. *Appl Spectrosc Rev* 2007;**42**:493-541.
 44. Nemecek D, Stepanek J, Thomas Jr GJ. Raman spectroscopy of proteins and nucleoproteins. *Curr Protoc Protein Sci* 2013;**17**:Unit17.8.
 45. Ilaslan K, Boyaci IH, Topcu A. Rapid analysis of glucose, fructose and sucrose contents of commercial soft drinks using Raman spectroscopy. *Food Control* 2015;**48**:56-61.
 46. Liu F, Gu H, Yuan X, et al., editors. Chloride ion-dependent surface-enhanced Raman scattering study of biotin on the silver surface. *J Physics: Conference Series*; 2011: IOP Publishing.
 47. Uusitalo S, Popov A, Ryabchikov YV, et al. Surface-enhanced Raman spectroscopy for identification and discrimination of beverage spoilage yeasts using patterned substrates and gold nanoparticles. *J Food Eng* 2017;**212**:47-54.
 48. Antoni D, Burckel H, Josset E, Noel G. Three-dimensional cell culture: a breakthrough in vivo. *Int J Mol Sci* 2015;**16**:5517-27.
 49. Scarritt ME, Pashos NC, Bunnell BA. A review of cellularization strategies for tissue engineering of whole organs. *Front Bioeng Biotechnol* 2015;**3**:43.
 50. Tamai M, Adachi E, Tagawa Y-i. Characterization of a liver organoid tissue composed of hepatocytes and fibroblasts in dense collagen fibrils. *Tissue Engineering Part A* 2013;**19**:2527-35.
 51. Kawasaki T, Kirita Y, Kami D, et al. Novel detergent for whole organ tissue engineering. *J Biomed Mater Res A* 2015;**103**:3364-73.
 52. Ma J, Ju Z, Yu J, et al. Decellularized Rat Lung Scaffolds Using Sodium Lauryl Ether Sulfate for Tissue Engineering. *ASAIO J* 2018;**64**:406-14.
 53. Soto-Gutierrez A, Zhang L, Medberry C, et al. A whole-organ regenerative medicine approach for liver replacement. *Tissue Eng Part C Methods* 2011;**17**:677-86.
 54. Wang Y, Cui CB, Yamauchi M, et al. Lineage restriction of human hepatic stem cells to mature fates is made efficient by tissue-specific biomatrix scaffolds. *Hepatology* 2011;**53**:293-305.
 55. Yu C, Ma X, Zhu W, et al. Scanningless and continuous 3D bioprinting of human tissues with decellularized extracellular matrix. *Biomaterials* 2019;**194**:1-13.
 56. Mazza G, Rombouts K, Hall AR, et al. Decellularized human liver as a natural 3D-scaffold for liver bioengineering and transplantation. *Sci Rep* 2015;**5**:13079.
 57. Takeda YS, Xu Q. Fabrication of 2D and 3D constructs from reconstituted decellularized tissue extracellular matrices. *J Biomed Nanotechnol* 2014;**10**:3631-7.
 58. Lorvellec M, Scottoni F, Crowley C, et al. Mouse decellularised liver scaffold improves human embryonic and induced pluripotent stem cells differentiation into hepatocyte-like cells. *PLoS one* 2017;**12**:e0189586.
 59. Li Y, Wu Q, Wang Y, et al. Construction of bioengineered hepatic tissue derived from human umbili-

- cal cord mesenchymal stem cells via aggregation culture in porcine decellularized liver scaffolds. *Xenotransplantation* 2017;**24**:e12285.
60. Coronado RE, Somaraki-Cormier M, Natesan S, *et al*. Decellularization and Solubilization of Porcine Liver for Use as a Substrate for Porcine Hepatocyte Culture: Method Optimization and Comparison. *Cell Transplant* 2017;**26**:1840-54.
 61. Lin P, Chan WC, Badylak SF, Bhatia SN. Assessing porcine liver-derived biomatrix for hepatic tissue engineering. *Tissue Eng* 2004;**10**:1046-53.
 62. Pan MX, Hu PY, Cheng Y, *et al*. An efficient method for decellularization of the rat liver. *J Formos Med Assoc* 2014;**113**:680-7.
 63. Yang X, Wang X, Huang X, *et al*. A hybrid co-culture model with endothelial cells designed for the hepatic tissue engineering. *J Mater Sci Mater Med* 2017;**28**:139.
 64. Bale SS, Geerts S, Jindal R, Yarmush ML. Isolation and co-culture of rat parenchymal and non-parenchymal liver cells to evaluate cellular interactions and response. *Sci Rep* 2016;**6**:25329.
 65. Kim K, Ohashi K, Utoh R, *et al*. Preserved liver-specific functions of hepatocytes in 3D co-culture with endothelial cell sheets. *Biomaterials* 2012;**33**:1406-13.
 66. Bhandari RN, Riccalton LA, Lewis AL, *et al*. Liver tissue engineering: a role for co-culture systems in modifying hepatocyte function and viability. *Tissue Eng* 2001;**7**:345-57.
 67. Thomas RJ, Bhandari R, Barrett DA, *et al*. The effect of three-dimensional co-culture of hepatocytes and hepatic stellate cells on key hepatocyte functions in vitro. *Cells Tissues Organs* 2005;**181**:67-79.